IST Contributions to the ASDEX Upgrade Edge and Divertor Physics Using Microwave Reflectometry

C Silva, D Aguiam, M Bernert, G D Conway, L Gil, B Gonçalves, L Guimarais, T Happel, Stéphane Heuraux, P Manz, et al.

IST CONTRIBUTIONS TO THE ASDEX UPGRADE EDGE AND DIVERTOR PHYSICS USING MICROWAVE REFLECTOMETRY

C. SILVA[1], D. AGUIAM[1], M. BERNERT[2], G. D. CONWAY[2], L. GIL[1], B. GONÇALVES[1], L. GUIMARAIS[1], T. HAPPEL[2], S. HEURAUX[3], P. MANZ[2], M. E. MANSO[1], V. NIKOLAEVA[1], J. SANTOS[1], E. SELIUNIN[1], A. SILVA[1], F. DA SILVA[1], U. STROTH[2], J. VICENTE[1], E. WOLFRUM[2] AND THE ASDEX UPGRADE TEAM AND THE EUROFUSION MST1 TEAM*

[1]Instituto de Plasmas e Fusão Nuclear, Instituto Superior Técnico, Universidade de Lisboa, Portugal
[2]Max-Planck-Institut fur Plasmaphysik, Boltzmannstr. 2, 85748, Garching, Germany
[3]Institut Jean Lamour, UMR 7198, CNRS-U. de Lorraine, BP 50840, F-54011 Nancy cedex, France
*See the author list of Meyer H. et al 2017 Nucl. Fusion 57 102014
Email of corresponding author: csilva@ipfn.tecnico.ulisboa.pt

Abstract

Information of the plasma density such as provided by reflectometry is essential for the study and operation of magnetically confined fusion devices. The microwave reflectometry systems developed by IST for ASDEX Upgrade consist of: (i) a multi-band frequency modulated continuous wave O-mode reflectometer with the unique capability of providing profile and fluctuations measurements on the high-field side and low-field side (LFS) simultaneously, making it a relevant diagnostic for poloidal asymmetry studies; (ii) a fast frequency hopping O-mode reflectometer used to obtain more detailed information on density fluctuations at the LFS; and (iii) a multichannel X-mode reflectometry diagnostic recently installed to measure the edge density profile in front of the ICRF antenna. This contribution presents an overview of the scientific results obtained with the different reflectometry systems used in a complementary way in order to address some of the key issues under investigation at ASDEX Upgrade. The experimental results obtained demonstrate that the IST reflectometry systems provide a valuable contribution to a better understanding of important physics topics such as connection between midplane and divertor conditions, dynamics of the density profiles, SOL turbulence, pedestal instabilities, RF sheath effects and real-time control.

1. INTRODUCTION

Information of the plasma density is essential for the study and operation of magnetically confined fusion devices. Microwave reflectometry appears as an attractive diagnostic due to its high temporal and spatial resolution and its application to profile as well as fluctuation density measurements.

The microwave reflectometry systems developed by IST for ASDEX Upgrade (AUG) consist of: (i) a multi-band frequency modulated continuous wave (FM-CW) O-mode reflectometer with the unique capability of providing profile and fluctuations density measurements on the high-field side (HFS) and low-field side (LFS) simultaneously, making it a relevant diagnostic for poloidal asymmetry studies; (ii) a fast frequency hopping O-mode reflectometer used to obtain more detailed information on density fluctuations at the LFS; and (iii) a multichannel X-mode reflectometry diagnostic recently installed to measure the edge density profile in front of the ICRF antenna. This contribution presents an overview of the scientific results obtained with the different reflectometry systems used in a complementary way in order to address some of the key issues under investigation at AUG.

2. INFLUENCE OF THE HIGH-FIELD SIDE DENSITY FRONT ON THE MIDPLANE DENSITY PROFILES

The separatrix density and the scrape-off layer (SOL) conditions have a significant impact on the pedestal stability and hence on plasma confinement. However, the physics mechanisms responsible for the changes in confinement with fuelling, input power and impurity seeding have not yet been fully identified. Our main goal is to clarify the impact of the region of high density in the inner divertor (HFSHD) on the H-mode midplane profiles following a previous work for L-mode plasmas [1].

To explore the effect of fuelling and input power a discharge with steps in these quantities is analysed. Fig. 1 displays the evolution of the LFS separatrix density, $n_{e,sep}$, and HFS density just in front of the inner wall, $n_{e,wall}$, both estimated from reflectometry, together with that of the main discharge parameters. At the LFS, the edge density at the midplane is observed to respond clearly to the increase in the fuel rate leading to an outward shift of the density profile. This is mainly seen by the increase in LFS separatrix density. On the contrary, the input power has a minor impact on the density profile at the LFS with no changes observed in $n_{e,sep}$ when the power is

stepped-up. At the HFS, an HFSHD is observed to exist at the midplane from early in the discharge (t < 1.5 s) as consequence of the relatively high input power and line-averaged density. The density measured by reflectometry just in front of the inner vessel wall, follows closely the temporal evolution of the HFSHD in the divertor region. The density gets stronger when the gas input is raised at t = 2.5 s and augments strongly when the input power is stepped up, close to t = 4 s. The effect of the input power is therefore clearly different at LFS and HFS, as it strongly increases the HFS density while the LFS profiles are not significantly modified.

Plasma confinement is also differently influenced by the variation in input power and fuelling (see Fig. 1). The normalized confinement time is observed to improve slightly (5 - 10%) when the power is stepped up and to degrade when the fuel rate is increased, corresponding to a different dependence on the plasma parameters than that observed for the HFSHD, which increases with both input power and fuelling. Results presented here confirm the existence of a relationship between plasma confinement, the shift in the midplane LFS density profile and the presence of the HFSHD with respect to changes in fuelling as previously reported [2]. However, the detrimental effect of the HFSHD on confinement was not visible in the discharges analyzed here with variations in the heating power. This suggests that more is at play with respect to the effect of the HFSHD in confinement. The presence of the HFSHD may be responsible for the relative shift of temperature and density profiles, causing a reduction in MHD stability. However, this detrimental effect is probably overcompensated by the positive effect of increasing the heating power on energy confinement.

The link between the HFSHD, divertor conditions and midplane density profiles is further explored by analysing the neutral pressure data measured by baratrons below the inner and outer divertor, Fig. 1. As the deuterium fuelling is raised, both the outer divertor neutral pressure and the LFS separatrix density increase confirming previous observations [3]. On the contrary, when the input power is raised neither the divertor neutral pressure in the outer target nor the midplane LFS separatrix density are significantly modified. Concerning the inner divertor, when deuterium fuelling is raised both the inner divertor neutral pressure and the SOL density at the HFS midplane increase, similarly to the observation at the LFS. However, when the input power is raised both the inner divertor neutral pressure and the SOL density at the HFS midplane increase contrary to the observed at the LFS. The evolution of the inner divertor neutral pressure is consistent with that of the HFSHD as both are seen to increase with fuelling and input power. Neutral pressure data gives further evidence that the LFS density profile is mainly influenced by the outer divertor target. An increase in the input power leads to a strong increase of the neutral pressure at the inner target and to a strengthening of the HFSHD but has a modest influence at the LFS (both at the midplane and outer divertor). In summary, our results indicate that the separatrix density at the LFS is better correlated with the neutral pressure at the outer target while the HFS SOL density follows the neutral pressure at the inner divertor.

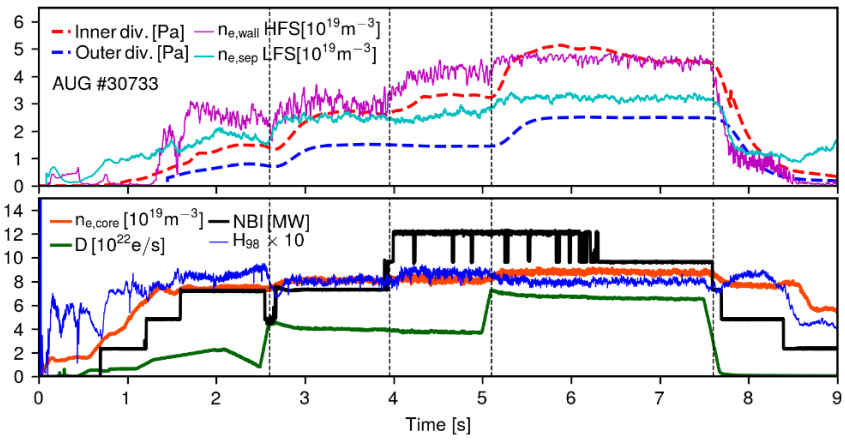

Fig. 1. Top: Evolution of the neutral pressure measured by the baratrons at the inner and outer divertor together with that of the LFS separatrix density, $n_{e,sep}$, and HFS density just in front of the inner wall, $n_{e,wall}$, both estimated from reflectometry. Bottom: Line-averaged core density, fuelling rate, NBI heating power and H_{98} for discharge #30733.

3. HFS/LFS EDGE TURBULENCE IN DIFFERENT STATES OF DIVERTOR DETACHMENT

Transport in the SOL depends on the state of the divertor detachment. It is also widely accepted that SOL/edge properties are not poloidally symmetric and therefore data from the under-diagnosed HFS is essential to improve the understanding of SOL transport and its link to the divertor conditions. To fill that gap, density fluctuations were measured simultaneously at the LFS and the HFS with the AUG FM-CW reflectometry system operating in

fixed frequency in plasmas where the state of divertor detachment evolves from attached to completely detached along density ramp L-mode discharges. Fluctuations are probed at three fixed density plasma layers that vary in radial position along the discharge following the dynamics of the plasma density profile. Density profiles at both the HFS and the LFS were also measured in paired discharges with the same FM-CW diagnostic operating in swept frequency enabling to localize the density layers where fluctuations are being measured at each probed time interval along the discharge.

The radial profiles of the density fluctuations level ($\delta n_e/n_e$) at the HFS and the LFS are displayed in Fig. 2. Also displayed in the figure is the fluctuation amplitude obtained by Langmuir probes at the LFS midplane in similar experimental conditions. The density fluctuation levels from reflectometry increase radially at both the LFS and the HFS as it is typically observed in fusion plasmas. The values of $\delta n_e/n_e$ at the HFS SOL are lower than at the LFS (by a factor of ≈ 2), which is consistent with ballooned transport. Density fluctuations from reflectometry at the LFS far-SOL matches quite well the Langmuir probe results (taking into account that $\delta n_e/n_e$ by the reciprocating probe were estimated from the ion saturation current measurements ignoring the contribution of temperature fluctuations).

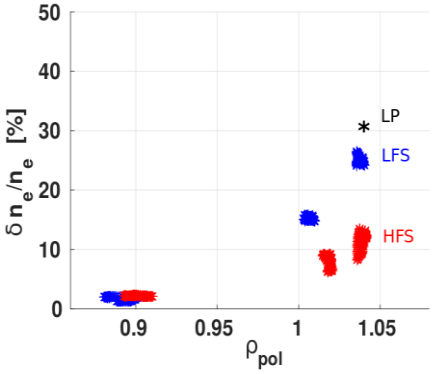

Fig. 2. Radial profiles of $\delta n_e/n_e$ at the LFS and the HFS obtained from FM-CW reflectometry in discharge #33484 with an edge line-averaged density of $n_e \approx 1.3\ 10^{19}\ m^{-3}$. The value of $\delta n_e/n_e$ estimated from the Langmuir probe data at the LFS midplane in similar experimental conditions is also indicated. Published in [4].

The relative density fluctuations at the LFS and HFS along different divertor states (in a density ramp discharge) are depicted in Fig. 3 revealing strong poloidal asymmetries of the SOL/edge midplane turbulence. Also it is seen that $\delta n_e/n_e$ changes differently along the discharge with radius. At the LFS, density fluctuations close to the separatrix (at ρ_{pol} =1.00-1.01 and ρ_{pol}=1.05), present a modest variation with increasing background density, also seen in the reciprocating Langmuir probe data (measuring around ρ_{pol}=1.05), while at $\rho_{pol}\approx$1.04 density fluctuations increase along the density ramp. In the last part of the discharge, during the complete detachment state, the reflected signals reveal that the increase of density fluctuation levels results mainly from an increase of the low frequency components (< 15 kHz), which is also observed in the Langmuir probe data. This is in agreement with the generally accepted view that radial transport at the LFS SOL is dominated by filamentary activity. Experimental results are in line with an enhanced convection of filaments that has been reported before [6] at the LFS at the beginning of the outer divertor detachment leading to a flatter edge/SOL density profile.

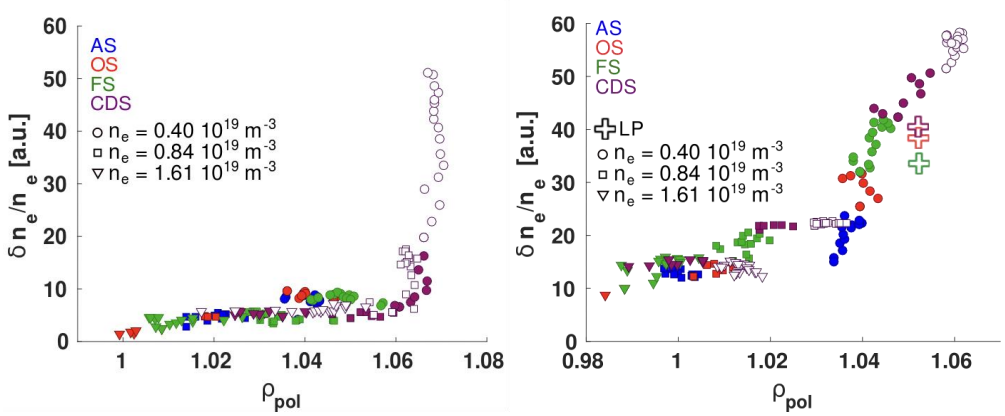

Fig. 3. Radial profiles of $\delta n_e/n_e$ obtained from the homodyne signal of the FM-CW reflectometer at HFS (left) and LFS (right) for discharge #33484. Color of points corresponds to the different divertor states according to [5]: attached (blue), onset (red), fluctuating (green) and complete detachment state (purple). Symbols correspond to different probed densities: $n_e = 0.40 \times 10^{19}\ m^{-3}$ (circles), $0.84 \times 10^{19}\ m^{-3}$ (squares) and $1.61 \times 10^{19}\ m^{-3}$ (triangles). Adapted from [4].

At the HFS a much lower level of fluctuations than at the LFS is observed at the midplane for all the divertor states, in agreement with ballooned transport. A strong increase of density fluctuations is seen at the far-SOL associated with filaments at the LFS becoming faster and less frequent. The increase of $\delta n_e/n_e$ at the HFS cannot be attributed to an increase of the local radial transport but rather to the presence of filaments that propagate parallel to the magnetic field lines from the LFS to the HFS. This study using HFS/LFS reflectometry measurements provides a consistent picture of the poloidal asymmetry in the density fluctuations and reveals that the divertor conditions influence significantly the midplane turbulence.

4. EDGE INSTABILITIES ACROSS THE L-H TRANSITION AND IN H-MODE

The L-H transition in AUG is often accompanied by the appearance of edge coherent modes (CMs) [7] or quasi-coherent modes (QCMs) [8] in density fluctuations. QCMs have also been detected in other devices [e.g. 9-10], including during ELM cycles. The underlying instabilities of these modes are mostly an open question, despite their relevance for understanding edge transport and pedestal physics.

Slow power ramp shots at different densities ($\overline{n_e}_{L-I}$ = 2.3, 4.0 and 4.6 $\times 10^{19}$ m^{-3}) have been conducted in AUG to study edge instabilities across the L-H transition and in H-mode, including the intermediate I-phase [10]. A lower single null configuration with B×∇B towards the X-point, constant deuterium gas puff and central ECRH power steps were used. Fig. 4 shows an overview of the medium density shot, in which the plasma undergoes an I-phase from 2.1 to 2.5 s with confinement improvement, as seen in the line-averaged electron density traces (Fig. 4(c)). Instabilities start to develop during this period and their amplitude grows and saturates when the plasma enters the ELM-free H-mode, as shown in the reflectometry phase (Fig. 4(a)) and radial magnetic field (Fig. 4(b)) spectrograms, which feature strong edge CMs with a multi-peak structure from 50 to 80 kHz. These have toroidal and poloidal mode numbers n = -(2-8) and m = 16-64, with propagation in the electron diamagnetic direction in the lab frame. Similar modes have been previously observed in AUG [8] and they are also present in the low density shot, but not in the high density one. After a few ELMs with which the CMs disappear and reappear, the plasma enters a very long ELM-free phase without impurity accumulation, lasting from 3.3 to 4.1 s and appearing to approach stationarity (see Fig. 4(c)), being only interrupted by NBI. The CMs are not present, but a broader QCM is visible in the reflectometry spectrogram of Fig. 4(a), with a down-chirping frequency from 60 to 35 kHz. It also exists in the high density shot, but not in the low density one and it is not visible in any magnetic signal. The high density QCM has n = 20-23, being smaller and slower than the low density CMs.

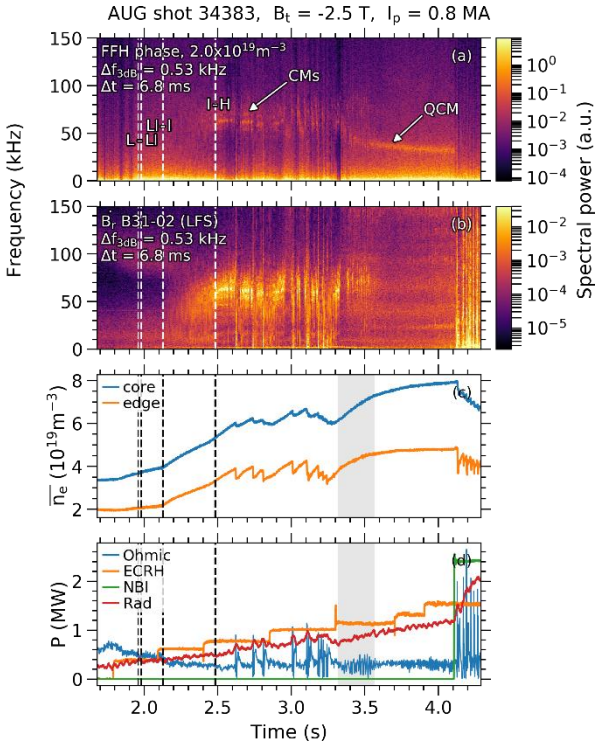

Fig. 4. Time traces from an L-H transition experiment: (a) spectrogram of reflectometry phase; (b) spectrogram of radial magnetic field coil; (c) line-averaged electron density; (d) heating and radiated power. The vertical dashed lines indicate the time instants of L-I-H transitions.

Between the phases with the CMs and QCM there is a period of alternation between the two modes (shaded region in Fig. 4), which is correlated with changes in several edge and divertor parameters. Whenever the QCM appears, temperature and density decrease in the edge and increase with a small time delay in the divertor. This suggests that the QCM causes an increase of transport in the pedestal, expelling plasma to the divertor. This may explain the absence of impurity accumulation and ELMs, as the increased transport could prevent the edge gradients from reaching the peeling-ballooning instability boundary. If so, these observations may open the door to an ELM-free regime at AUG which will be the subject of future experiments.

To sum up, edge instabilities with a complex time evolution after the L-I-H transition have been observed in AUG. Their type and behavior is different for the low and high density branches of the L-H power threshold and they may play an important role in the H-mode pedestal structure, stability and confinement.

5. UNDERSTANDING DENSITY PROFILES IN FRONT OF THE ICRH ANTENNA

A new multichannel reflectometer diagnostic was recently installed in an ICRF antenna, aiming mainly for ICRF coupling and operation studies [12]. The diagnostic has been implemented and successfully commissioned. One of the most challenging tasks of the diagnostic was the implementation of an automatic initialization of the X-mode upper cutoff measurement, which is the main source of error in X-mode density profile reconstruction. Two first fringe estimation algorithms were developed [12]: one based on amplitude and spectral information and another one using a neural network model to recognize the first fringe location from spectrogram data. The experimental density profile measurements were validated against other existing diagnostics on AUG. Based on the profile data, the high radial and poloidal sensitivity of the diagnostic has been demonstrated by tracking a vertical displacement of a circular plasma. The experimental density profiles were used to corroborate ICRH power coupling simulations under different gas puffing conditions and to observe poloidal convective transport during ICRH operation, taking advantage of the multichannel topology and its sensitivity to local plasma perturbations. RF sheaths formed during ICRF operation are believed to promote convective transport associated with the potential map in front of the ICRH antenna that influence power coupling as observed using the simultaneous reflectometry density profile measurements at the top, middle and bottom regions of the ICRF antenna [13].

This new reflectometry system opens up new research opportunities in the area of SOL physics by exploring the high temporal and spatial resolution of the diagnostic and by taking advantage of the three channels installed at different poloidal locations. In addition to the density profile measurements, the system is also being validated as a diagnostic tool for density fluctuations measurements [14], particularly relevant in the far-SOL that is generally inaccessible to the FW-CW reflectometer. The electron density profiles measured by different diagnostics, such as Langmuir probes mounted on the midplane manipulator (MEM), the lithium beam diagnostic (LiB) and multichannel reflectometer diagnostic (RIC) are compared in Fig. 5 for discharge #34290. Two time periods with $n_{e,core}$ = 3.3×10^{19} m^{-3} (left) and 5.0×10^{19} m^{-3} (right) are presented. Solid lines correspond to mean density profiles while dashed lines correspond to 2 times the standard deviation (σ) of the fluctuations above and below the mean profiles. As illustrated in Fig. 5, both the averaged SOL density and the amplitude of the fluctuations increase with core density as expected. A good agreement is observed between the profiles from the RIC, probes and LiB for both periods. RIC median ± 2σ profiles fit reasonably well the upper and lower boundaries of MEM density profiles and may represent the impact of fluctuation activity in the plasma profiles.

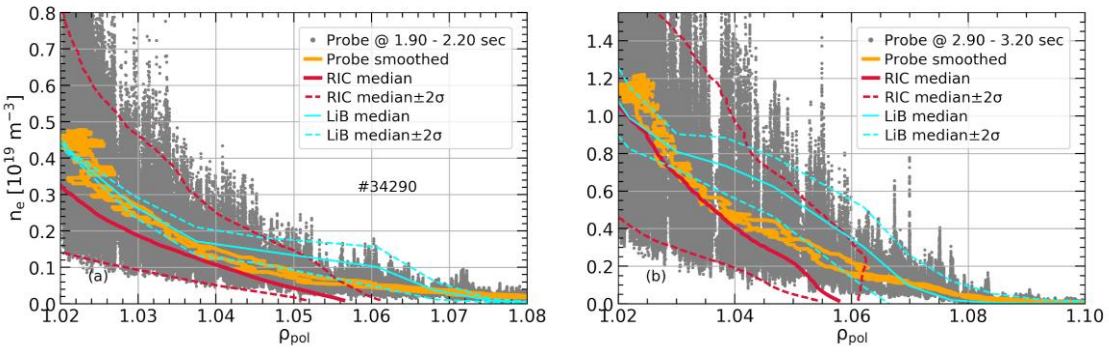

Fig. 5. Electron density profiles averaged over 10ms for discharge #34290 at two time periods, corresponding to $n_{e,core}=3.3\times10^{19}$ m^{-3} (a) and $n_{e,core}=5.0\times10^{19}$ m^{-3} (b). Dashed curves indicate the median ± 2σ profiles.

Differences in the amplitude of the fluctuations between the used diagnostics are most probably related with their different temporal resolutions, with larger fluctuations amplitudes naturally obtained for probes (2 MHz) and modest values obtained with LiB (10 kHz). As the density is increased, a flattening of the SOL plasma density profile is observed to occur above a Greenwald fraction of about $f_{GW} = 0.45-0.5$, in good agreement with previous results, suggesting an enhancement of the SOL radial transport [6].

6. SYNTHETIC REFLECTOMETRY DIAGNOSTIC

Aiming to improve the understanding and interpretation of experimental results from reflectometry, a synthetic reflectometry diagnostic has been developed employing full-wave simulations. By modelling reflectometry diagnostics together with sophisticated plasmas models, a true synergy can be developed between the experimental and numerical work to improve the reliability and interpretation of turbulence measurements.

The state-of-the-art full-wave code REFMUL is based on a finite-difference time-domain method [15]. This two-dimensional code allows setting up synthetic reflectometers by modelling features such as transmission waveguides, metallic horn antennae or in-phase $I(t) = A(t)\cos(\varphi(t))$ and quadrature $Q(t) = A(t)\sin(\varphi(t))$ detection schemes, similar to what is implemented experimentally. The probed medium, the plasma itself, can be modelled using analytical descriptions (for instance using well known turbulence models that can be found in literature) or employing numerical results obtained from more realistic gyro-fluid turbulence codes such as the GEMR [16]. Both approaches are used to study relevant phenomena in fusion plasmas such as coherent filament-like density structures [17] or broadband turbulence [18]. One illustrative example is shown in Fig. 6 where a background plasma density is displayed together with the electric field component of a probing wave at one given time iteration of a full-wave Doppler simulation. In this figure, it is possible to distinguish multiple effects in the reflected probing beam that occur in both Doppler and conventional set-up, such as the main reflection near the cut-off layer, Bragg backscattering, beam splitting and forward-scattering effects which are put in evidence using oblique injection.

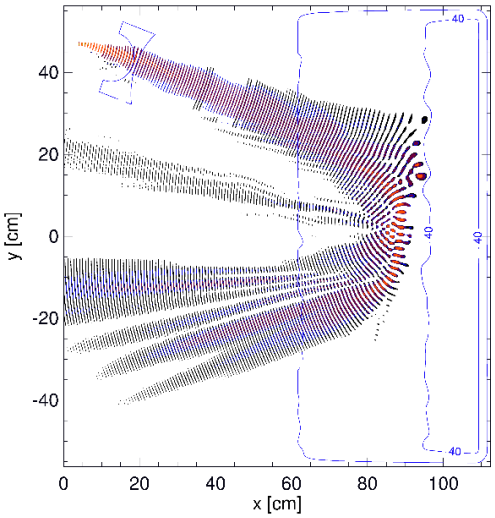

Fig. 6. Snapshot of a Doppler simulation showing the electric field E_z. The probing beam suffers forward-scattering, becoming fragmented.

REFMUL has been used, in particular, to model O-mode reflectometry diagnostics under different conditions of turbulence and infer plasma turbulence characteristics, such as the turbulence level, from the actual measurements. The evolution of reflectometry phase fluctuations with the plasma turbulence level ($\delta n_e/n_e$) is shown in Fig. 7 as an example. These results were obtained from simulations with Kolgomorov-like turbulence superimposed on a linear density profile. A linear relation between the phase and the turbulence level is observed only up to $\delta n_e/n_e \approx$ 2-4% followed by non-linear behavior at higher turbulence levels. The saturated phase response above a given turbulence level corresponds to a slight decrease in the reflected power and to the existence of non-linear physical phenomena in the plasma-wave interactions. The existence of non-linear response regimes of reflectometry stress the importance of numerical simulations in order to properly characterize the diagnostic response.

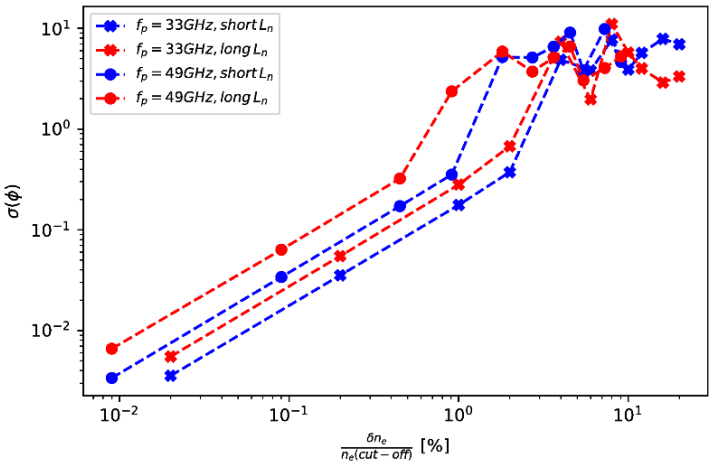

Fig. 7. Standard deviation of reflectometry φ(t) signals for turbulence level scans with 2 probing frequencies (33GHz and 49GHz) and 2 density gradient scale lengths L_n. Published in [17].

7. REAL-TIME PLASMA POSITION CONTROL

O-mode microwave reflectometry will be used on ITER and foreseeably on DEMO to complement the standard magnetic diagnostics for plasma position control. After a successful validation of the control scheme at the LFS in 2011 [19], the FMCW system at AUG continues to be used as a test ground for the development of this novel control technique, namely the real-time diagnostic infrastructure was upgraded to produce a demonstration at both HFS and LFS by generating the geometric plasma radius in real-time (RT). The system was successfully tested in standard regimes and also in plasmas developing an HFS density front were the validation assumptions of the technique are violated. Reflectometry's RT inner, R_{in}, and outer, R_{aus}, separatrix positions were combined to produce an approximation of the geometric plasma radius, $R_{geo} = (R_{in} + R_{aus})/2$, that was used to replace the corresponding magnetic measurement normally used as the position controller input signal.

Fig. 8 shows the main time traces of one of the 4 control discharges performed during 2016 experimental campaign. The top plot shows the core line-averaged density (H1), deuterium fuelling (D), NBI and ECRH heating power and plasma current (I_p). During the flat-top phase of the ELMy H-mode discharge, position control is handed to the reflectometry based controller from t ≈ 2.6 s until t ≈ 7.6 s, when the magnetic controller recover the control to perform the plasma ramp down.

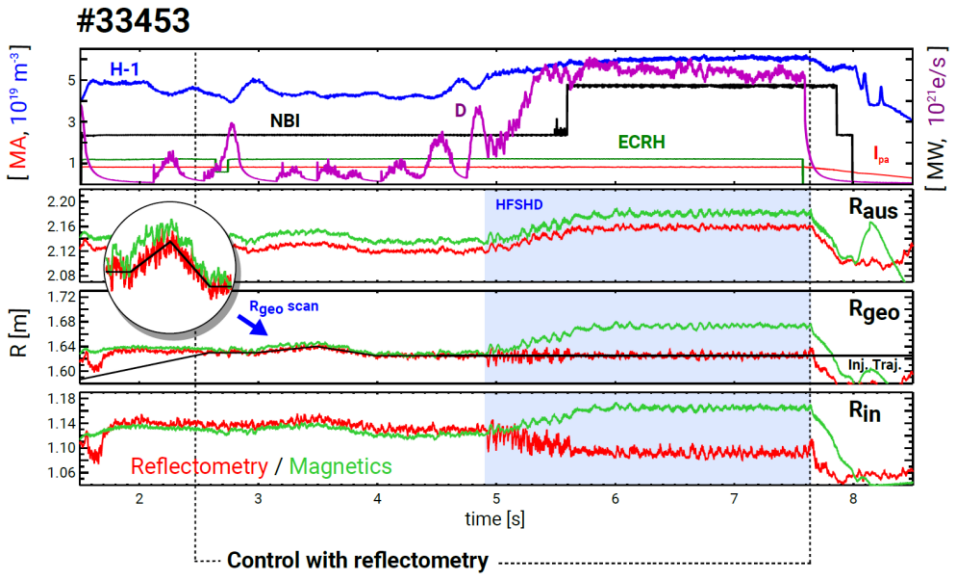

Fig. 8. Control of plasma position using R_{geo} (target inject trajectory in black). Position controller using reflectometry R_{geo} approximation switched on during t = [2.6 .. 7.6]s. From t=4.9s until t=8 s a HFSHD front appears.

During the reflectometry control phase, the geometric radius of the plasma column was programmed to swing 1.5cm (non-symmetrically) around its original position. As can be seen the new controller maintained reflectometry's R_{geo} within $\approx \pm 0.5$ cm of the target trajectory. Reflectometry estimates for R_{in}, R_{aus}, and R_{geo} are coherent with their magnetic counterparts, demonstrating very good precision. Input R_{geo} offsets were successfully handled by the position controller when switching to and from reflectometry input at $t \approx 2.6$s and $t \approx 7.6$s. From $t \approx 4.9$s to $t \approx 8$s a HFSHD front develops breaking the validity assumption of a constant density at flux-surfaces. During this period, the HFS separatrix position estimate is no longer valid and simply represents the position of a layer with a density similar to the one used to estimate the separatrix at the LFS. Reflectometry provided R_{geo} becomes then the mid-point position of the inner and outermost layers with densities equal to the expected density at the separatrix. In this period, the controller is acting as a gap controller rather than a replacement of a standard magnetic controller. In all four control discharges (#33448, #33450, #33452 and #33453) the system operated flawlessly during the complete programmed reflectometry control phases. The uninterrupted stream of control R_{geo} estimates, produced every 1 ms, reach the DCS with a total latency always < 350 μs proving that the developed system could be operated in much faster (3x) control cycles.

8. SUMMARY

Experimental results demonstrate that the IST reflectometry systems at AUG provide a valuable contribution to a better understanding of important physics issues such as pedestal instabilities, SOL turbulence, dynamics of the density profiles and the connection between midplane and divertor conditions. Different upgrades are under development, to improve the temporal resolution and to expand the measuring density range of the FM-CW system that will provide uniquely versatile diagnostics for combined profile and fluctuations measurements particularly relevant for edge instabilities and turbulence studies.

ACKNOWLEDGEMENTS

This work has been carried out within the framework of the EUROfusion Consortium and has received funding from the Euratom research and training programme 2014-2018 under grant agreement No 633053. IST activities also received financial support from "Fundação para a Ciência e Tecnologia" through project UID/FIS/50010/2013. The views and opinions expressed herein do not necessarily reflect those of the European Commission.

REFERENCES

[1] L. GUIMARAIS et al, Nucl. Fusion 58 026005D 2018
[2] M.G. DUNNE et al, Plasma Phys. Control. Fusion 59 014017 2017
[3] A. KALLENBACH et al., Plasma Phys. Control. Fusion, 60 045006 2018
[4] V. NIKOLAEVA et al, Plasma Phys. Control. Fusion 60 055009 2018
[5] S. POTZEL et al, Nucl. Fusion 54 013001 2014
[6] D. CARRALERO et al, Nucl. Fusion 54 123005 2014
[7] A. MEDVEDEVA et al., Plasma Phys. Control. Fusion 59 125014 2017
[8] S. DA GRAÇA et al, EPS Conference on Plasma Physics 2013
[9] H.Q. WANG et al, Phys. Rev. Lett. 112 185004 2014
[10] A. DIALLO et al, Nucl. Fusion 55 053003 (2015)
[11] L. GIL et al, EPS Conference on Plasma Physics 2018
[12] D. AGUIAM et al, Rev. Sci. Instrum. 87 11E722 2016
[13] W. ZHANG et al, Nucl. Fusion 57 116048 2017
[14] E. SELIUNIN et al, EPS Conference on Plasma Physics 2018
[15] F. DA SILVA at al, J. Comput. Phys. 203 467 2005
[16] B.D. SCOTT, Physics of Plasmas 12 102307 2005
[17] J. VICENTE et al, Rev. Sci. Instrum. 85 11D817 2014
[18] J. VICENTE et al, Rev. Sci. Instrum. 89 10H110 2018
[19] J. SANTOS et al, Nucl. Fusion 52 032003 2012